ACS APPLIED MATERIALS & INTERFACES

Research Article

www.acsami.org

One-Step Synthesis of Water-Soluble MoS_2 Quantum Dots via a Hydrothermal Method as a Fluorescent Probe for Hyaluronidase Detection

Wei Gu, Yinghan Yan, Cuiling Zhang,* Caiping Ding, and Yuezhong Xian*

Shanghai Key Laboratory of Green Chemistry and Chemical Processes, Department of Chemistry, School of Chemistry and Molecular Engineering, East China Normal University, 500 Dongchan Road, Shanghai 200241, China

Supporting Information

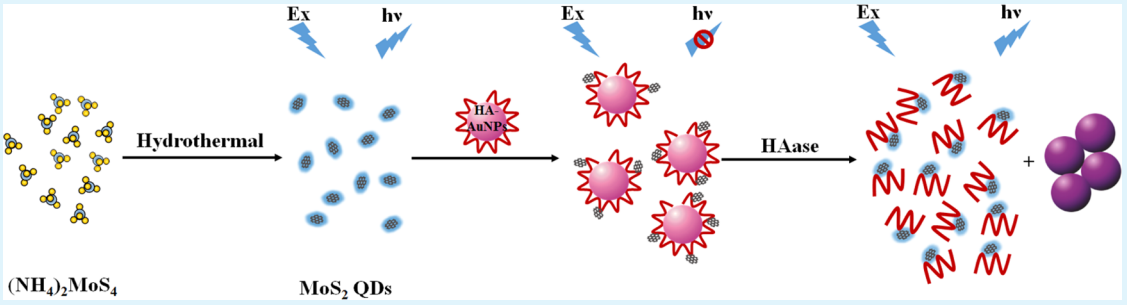

ABSTRACT: In this work, a bottom-up strategy is developed to synthesize water-soluble molybdenum disulfide quantum dots (MoS_2 QDs) through a simple, one-step hydrothermal method using ammonium tetrathiomolybdate [$(NH_4)_2MoS_4$] as the precursor and hydrazine hydrate as the reducing agent. The as-synthesized MoS_2 QDs are few-layered with a narrow size distribution, and the average diameter is about 2.8 nm. The resultant QDs show excitation-dependent blue fluorescence due to the polydispersity of the QDs. Moreover, the fluorescence can be quenched by hyaluronic acid (HA)-functionalized gold nanoparticles through a photoinduced electron-transfer mechanism. Hyaluronidase (HAase), an endoglucosidase, can cleave HA into proangiogenic fragments and lead to the aggregation of gold nanoparticles. As a result, the electron transfer is blocked and fluorescence is recovered. On the basis of this principle, a novel fluorescence sensor for HAase is developed with a linear range from 1 to 50 U/mL and a detection limit of 0.7 U/mL.

KEYWORDS: *MoS_2 quantum dots, hydrothermal method, fluorescence, biosensor, hyaluronidase*

1. INTRODUCTION

As one kind of layered two-dimensional (2D) nanomaterial, molybdenum disulfide (MoS_2) with 2D building blocks (S−Mo−S layers) weakly bound by van der Waals force has attracted great attention.[1,2] Because of its unique chemical, mechanical, and electronic properties,[3] MoS_2 is widely used as a lubricant and hydrogen evolution and photocatalytic material.[4] Recently, band-gap tuning of MoS_2 from an indirect-band-gap bulk material to a direct-gap semiconductor has been realized by adjusting the numbers of layers, and photoluminescence arising from the quantum confinement effect in d-orbital-related interaction in a MoS_2 monolayer is strong evidence of the band-gap transition.[5−7] Moreover, while the size of MoS_2 is controlled to be less than 10 nm, zero-dimensional MoS_2 quantum dots (QDs) can be synthesized. Because of quantum confinement and edge effects,[8,9] MoS_2 QDs possess unique optical and electronic properties and are potentially applicable in fluorescence sensing,[10] catalysis,[7,11] bioimaging,[12−15] etc.

To date, several strategies have been developed to synthesize MoS_2 QDs, generally including "top-down" and "bottom-up" routes. As for the "top-down" method, physicochemical strategies are used to engineer the size and dimension of layered bulk MoS_2 materials. Through a microexfoliation technique, monolayer MoS_2 nanosheets were obtained, and photoluminescence was reported for the first time in 2010.[9] After that, various exfoliation methods were developed to synthesize MoS_2 QDs.[7,11,16−20] For example, Stengl and Henych reportedly prepared MoS_2 QDs by refluxing the exfoliated single- or few-layered MoS_2 nanosheets in ethylene glycol.[16] Zhang et al. demonstrated the synthesis of monodisperse transition-metal dichalcogenide nanodots, including MoS_2 QDs, through a combination of grinding and sonication.[18] They declared that the shear/compress force of grinding and the high energy sonication were able to break up the covalent chemical bonds and disintegrate bulk crystals. Very recently, MoS_2 QDs with up-conversion and down-conversion properties were synthesized through a tetrabutylammonium-assisted sonication route.[14] As for these "top-down" approaches, hazardous reagent, organic solvent, or a long-time pretreatment are typically required. As for the "bottom-up"

Received: January 28, 2016
Accepted: April 15, 2016
Published: April 15, 2016

DOI: 10.1021/acsami.6b01166
ACS Appl. Mater. Interfaces 2016, 8, 11272−11279

Scheme 1. Schematic Representation of the Detection of HAase

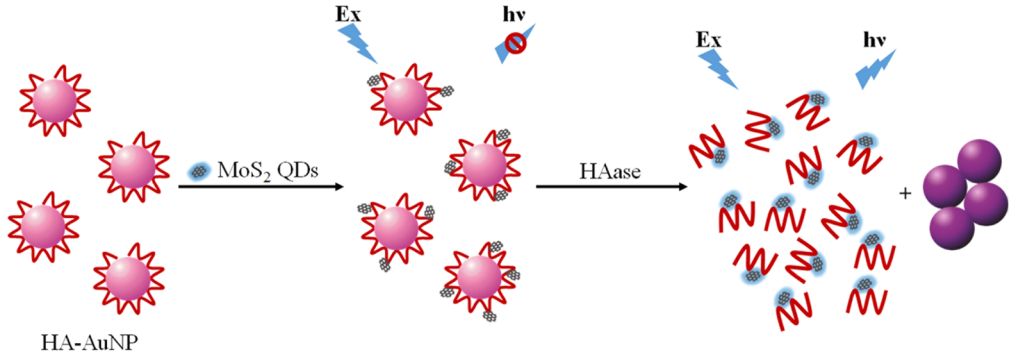

route, the size of the QDs can very easily be confined by controlling the chemical reaction conditions. For example, using DNA as the biotemplate, well-crystallized MoS_2 QDs were synthesized through a reaction between $MoCl_5$ and Na_2S in the DNA matrix. However, no photoluminescence was observed from the as-prepared nanoclusters.[21] Wang and Ni reportedly synthesized MoS_2 QDs using sodium molybdate and cysteine as precursors, and the obtained QDs were used as fluorescence probes for the detection of 2,4,6-trinitrophenol.[10] MoS_2 QDs with excellent hydrogen evolution activity were prepared by a hydrothermal route using sodium molybdate and dibenyl disulfides as Mo and S sources, respectively.[22] However, these methods may suffer from the formation of C dots during the high-temperature hydrothermal process. It is because the thiol-containing organic molecules may act as S and C sources simultaneously during the process of chemical reaction. Very recently, Lin et al. prepared MoS_2 QDs using ammonium tetrathiomolybdate as a precursor and oleylamine as a reducing agent. However, the resultant MoS_2 QDs are hydrophobic.[15] Even though the QDs could be transferred from an organic solvent to water with the help of cetyltrimethylammonium bromide (CTAB), it may result in a decrease in the quantum yield. In addition, CTAB is reported to possess cytotoxicity and is not suitable for biological applications. So far, the as-prepared MoS_2 QDs have been used as catalysts for hydrogen evolution reaction,[7,11,19,22] and the fluorescent probe has been used for bioimaging.[12,13,15] The synthesis and application of MoS_2 QDs in biosensors are in their preliminary stages and need to be further explored.[23]

Hyaluronidase (HAase) is an endoglucosidase that can cleave hyaluronic acid (HA),[24,25] a linear glycosaminoglycan with repeating D-glucuronic acid and *N*-acetyl-D-glucosamine disaccharide units,[26] into proangiogenic fragments. It has been reported that HAase is relevant to many physiological and pathological processes, for example, embryogenesis, inflammation, and wound healing.[27−31] Recently, overexpression of HAase was found in many malignant tumors, such as bladder,[32,33] prostate,[34] brain,[35] and colorectal[36] cancers. Thus, evaluation of the activity of HAase has drawn wide consideration because HAase might be a potential tumor marker. Especially, the development of sensitive HAase detection is of great importance for clinical diagnosis and therapy of cancer at its early stage. However, traditional detecting methods, such as viscosimetry,[37] turbidimetry,[38] colorimetry,[33,39,40] and zymography,[41] usually lack sensitivity and selectivity. Although immunoassay is very sensitive and selective for HAase detection,[42] expensive antibodies and tedious steps limited its application. A fluorescence technique is appropriate for HAase quantification because of its distinct advantages, such as ease of operation, high sensitivity, capability of real-time monitoring, and suitability for high-throughput screening. Generally, fluorophore-labeled HA is designed to form a donor−acceptor pair, and fluorescence of the fluorophore is quenched. In the presence of HAase, cleavage of the HA chain and recovery of fluorescence are realized.[43−46] Very recently, an up-conversion nanoprobe for HAase was developed through coupling of the HA-bearing up-conversion fluorescent nanoparticles with poly(*m*-phenylenediamine) nanospheres via covalent linkage.[47] Although these strategies were reported to investigate the activity of HAase, modification of the substrate was time-consuming and might affect the activity of HAase. In order to overcome these issues, a label-free fluorescent probe was developed to evaluate the bioactivity of HAase. For instance, Liu et al. developed a surface energy-transfer system between amino-functionalized C dots and HA-stabilized gold nanoparticles (AuNPs) for the detection of HAase based on its ability to degrade HA.[48] Compared with these HAase detection strategies using fluorophore-labeled HA, the label-free strategy is simple, flexible, and versatile. Thus, the development of label-free fluorescent HAase probes with high stability, selectivity, and sensitivity is urgent for bioactivity evaluation, clinical diagnosis, and early therapy.

In this study, we report a "bottom-up" strategy to prepare high-quality water-soluble MoS_2 QDs through hydrothermal reaction using ammonium tetrathiomoybdate $[(NH_4)_2MoS_4]$ as Mo and S sources. The as-prepared MoS_2 QDs were used to develop fluorescent probes for HAase using HA-functionalized AuNPs (HA-AuNPs) as fluorescence quenchers (shown in Scheme 1). In the nanoassembly of MoS_2 QDs/HA-AuNPs, the fluorescence of MoS_2 QDs was quenched by HA-AuNPs by photoinduced electron transfer (PET). With the addition of HAase, HA was cleaved into proangiogenic fragments, which led to dismantlement of the nanoassembly and aggregation of AuNPs due to the loss of protection from HA. Owing to the absence of quenchers (AuNPs) in the sensing system, fluorescence of MoS_2 QDs was recovered.

2. EXPERIMENTAL SECTION

2.1. Reagents and Chemicals. $(NH_4)_2MoS_4$ was obtained from J&K Chemical Ltd. (Shanghai, China). Hydrazine hydrate (N_2H_4, 85%), tetrachloroauric acid ($HAuCl_4$), sodium borohydride ($NaBH_4$), and sulfuric acid were purchased from Sinopharm Chemical Reagent Co. Ltd. (Shanghai, China). HA (from rooster comb) and HAase (400 U/mg) were purchased from Sigma-Aldrich. Quinine sulfate dehydrate (QS) were commercially available from Aladdin Industrial Co. Ltd. (Shanghai, China). PBS buffer (10 mM, pH 6.0) was employed in the

DOI: 10.1021/acsami.6b01166
ACS Appl. Mater. Interfaces 2016, 8, 11272−11279

experiment. Deionized distilled water was used throughout the experiment.

2.2. Characterization. Transmission electron microscopy (TEM) and high-resolution transmission electron microscopy (HRTEM) imaging was performed using a HT-7700 transmission electron microscope (Hitachi, Tokyo, Japan). Atomic force microscopy (AFM) images were recorded with tapping mode in air using a Dimension Icon atomic force microscope (Bruker, Karlsruhe, Germany). X-ray diffraction (XRD) pattern was characterized on a D8 Advance powder X-ray diffractometer (Bruker, Karlsruhe, Germany). X-ray photoelectron spectrometry (XPS) spectra were collected on an AXIS Ultra DLD X-ray photoelectron spectrometer (Shimadzu, Kyoto, Japan). UV−vis spectra were taken using an UV-2550 spectrophotometer (Shimadzu, Kyoto, Japan). Fluorescence spectra and fluorescence lifetime were recorded on a F-7000 fluorescence spectrometer (Hitachi, Tokyo, Japan) and a C11367 fluorescence lifetime spectrometer (Hamamatsu Photonics, Shizuoka, Japan), respectively. The dynamic light scattering (DLS) and ζ potentials were measured on Zetasizer Nano ZS90 nanoparticle size and zeta potential analyzers (Malvern Instruments, Malvern, U.K.).

2.3. Synthesis of MoS_2 QDs. The MoS_2 QDs were synthesized through a one-step hydrothermal route with $(NH_4)_2MoS_4$ as the precursor. In a typical procedure, $(NH_4)_2MoS_4$ was dispersed in 40 mL of water. After ultrasonication for 10 min, N_2H_4, as a reducing agent,[49] was added to the solution. Then, the mixture was transferred to a 50 mL poly(tetrafluoroethlene) (Teflon) autoclave and kept at 200 °C for 8 h. After being cooled to room temperature naturally, the mixture was filtered through a 0.22 μm microporous membrane, and the filtrate was purified by dialysis in water. After that, solid samples were obtained by evaporating the solvents.

2.4. Synthesis of HA-AuNPs. HA-AuNPs were synthesized by reported methods with minor modification.[46,50] In brief, 1.3 mL of $HAuCl_4$ (40 mg/mL) was dispersed in 50 mL of a HA sodium salt solution (0.1 mg/mL) with vigorous stirring. Then, 1 mL of $NaBH_4$ (4 mg/mL) was added to the mixture drop by drop, and the color of the mixture changed from yellow to red purple, indicating the formation of HA-AuNPs. Then, the solution was ultrafiltered with a 10 kDa ultrafiltration centrifuge tube. The purified HA-AuNP colloid was stored at 4 °C for further usage.

2.5. HAase Measurement. The general procedure for HAase analysis was performed as follows. In brief, 180 μL of HAase with different concentrations, 20 μL of MoS_2 QDs (0.5 mg/mL), and 40 μL of HA-AuNP colloids were added to 760 μL of PBS buffer. Then the mixture was incubated at 37 °C for 45 min, and the fluorescence emission spectra were recorded for quantitative analysis.

HAase in human urine samples was determined through the standard addition method. The urine sample was centrifuged for 20 min and mixed with different concentrations of HAase before measurement to prepare the spiked samples. The protein concentration of the urine sample was measured using Bio-Rad protein detection kits.

3. RESULTS AND DISCUSSION

3.1. Characterization of MoS_2 QDs. A typical TEM image of the resultant MoS_2 QDs (Figure 1A) shows that the QDs are well dispersed with a narrow lateral size distribution ranging from 1.5 to 4.5 nm. The average diameter is about 2.8 nm. The highly paralleled and ordered lattice fringe was observed in the HRTEM image (Figure 1B), confirming the high crystallinity of the MoS_2 QDs. The lattice fringe spacing is about 0.21 nm, which is in well agreement with the work of Gan et al.[51] The *d* spacing of the MoS_2 QDs matches well with the (006) lattice of the hexagonal crystal MoS_2.[12,52,53] AFM was performed to further investigate the morphology and thickness of the as-prepared QDs. As shown in Figure 1C, the thickness of the MoS_2 QDs ranges from 1.4 to 2.5 nm, demonstrating that the MoS_2 QDs are few-layered.[53] According to the theoretical monolayer thickness (about 0.7 nm) for the S−Mo−S

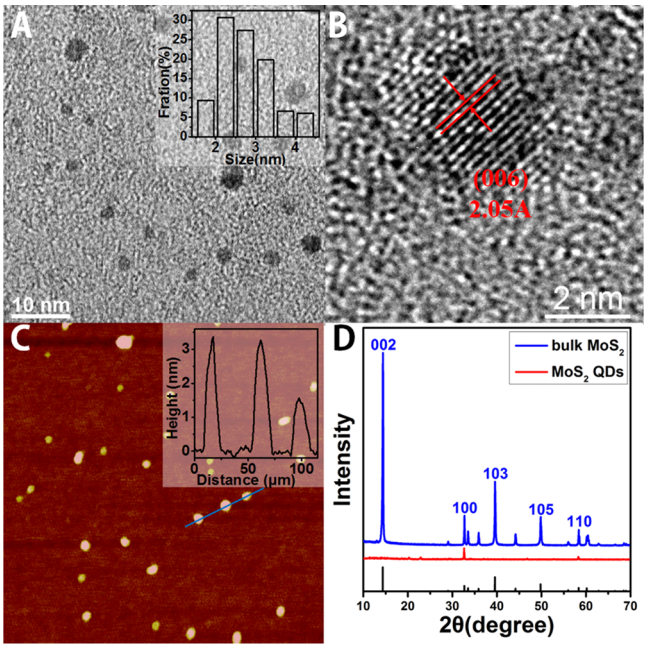

Figure 1. (A) TEM, (B) HRTEM, and (C) AFM images of the MoS_2 QDs. (D) XRD patterns of bulk MoS_2 (blue line), MoS_2 QDs (red line), and the standard MoS_2 (JCPDS card 37-1492; black line). The insets of parts A and C show the size and height distributions of the MoS_2 QDs, respectively.

structure,[18] the as-synthesized MoS_2 QDs are about 2−4 layers. Figure S1 shows the Raman spectrum of the MoS_2 QDs, and two Raman peaks can be observed at 380.9 and 405 cm^{-1}, corresponding to the in-plane (E^1_{2g}) and out-of-plane (A_{1g}) vibrations of the Mo−S bonds in 2H-MoS_2.[5] The frequency difference of those two peaks is about 24.1 cm^{-1}, indicating the thin-layer structure of the MoS_2 QDs.[54] This is well consistent with the result obtained from AFM measurement. The crystal structure was investigated through XRD with bulk MoS_2 as a reference. Compared to bulk MoS_2 (the blue line in Figure 1D), the (002) diffraction peak at 2θ = 14.4° disappears in the MoS_2 QDs, which is attributed to the thin-layer structure of the QDs.[11] Rao et al. also reported the disappearance of the characteristic (002) diffraction peak for monolayer MoS_2 nanosheets, which is due to the lack of interlayer action.[55] The two weak peaks at 2θ = 32.6° and 58.4° in the XRD pattern of the MoS_2 QDs are attributed to the (100) and (110) diffractions, respectively.

XPS measurements were performed to investigate the chemical state and composition of the QDs. As shown in the XPS spectrum of MoS_2 QDs (Figure S2), Mo and S could be detected and the atomic ratio of Mo:S was about 1:2.09, confirming the formation of MoS_2 QDs. As shown in the high-resolution Mo 3d spectrum (Figure 2A), two characteristic peaks at 229.3 and 232.5 eV belong to Mo^{IV} $3d_{5/2}$ and Mo^{IV} $3d_{3/2}$, respectively. This suggests that the dominance of Mo is the 4+ oxidation state.[7,11,19] The peaks around 226.6, 163.4, and 162.2 eV in Figure 2A,B are attributed to S 2s, S $2p_{1/2}$, and S $2p_{3/2}$ orbitals of divalent sulfide ions.[11,17,53] The small peaks located at 235.7 and 168.6 eV are ascribed to Mo^{6+} and S^{6+}, which may result from slight oxidation during the reaction process.[7]

3.2. Optical Features of MoS_2 QDs. Figure 3A shows the UV−vis spectrum of as-prepared MoS_2 QDs. We can see a shoulder peak located at 306 nm, which is assigned to the blue-

DOI: 10.1021/acsami.6b01166
ACS Appl. Mater. Interfaces 2016, 8, 11272−11279

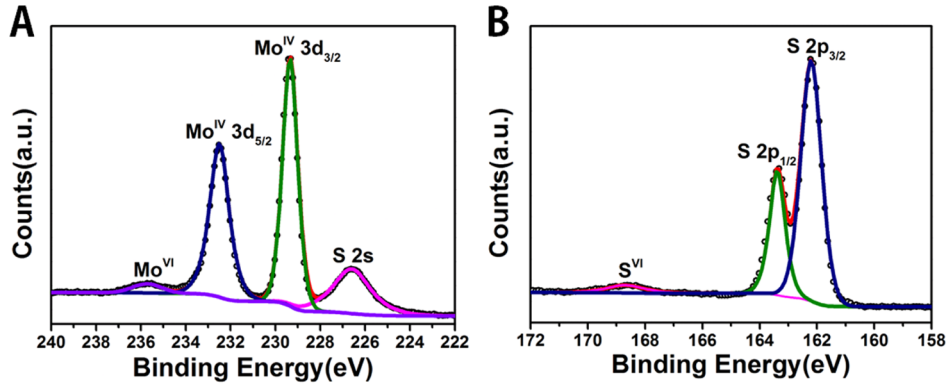

Figure 2. High-resolution peak-fitting XPS spectra of Mo^{IV} 3d (A) and S 2p (B).

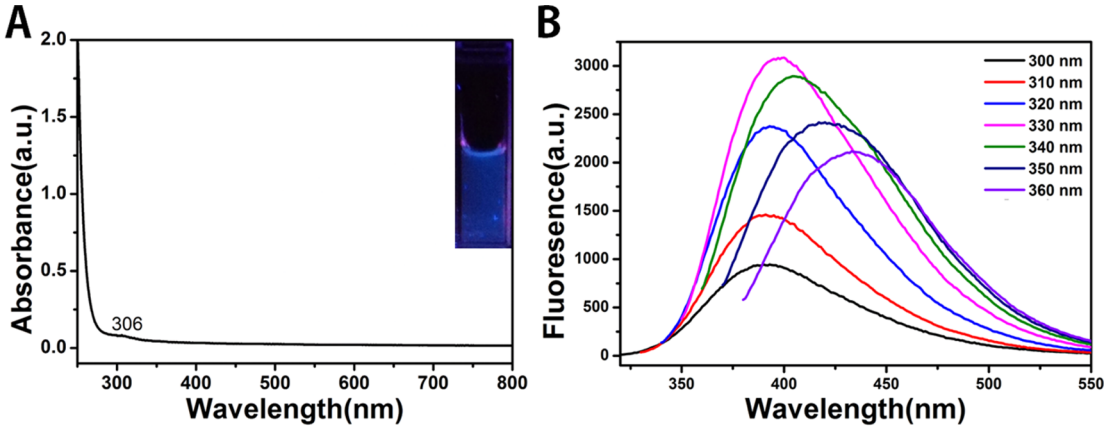

Figure 3. (A) UV−vis spectra of the MoS_2 QDs. The inset is a digital photograph of a QD aqueous solution (0.5 mg/mL) under UV light (365 nm). (B) Fluorescence emission spectra of the MoS_2 QDs at different excitation wavelengths.

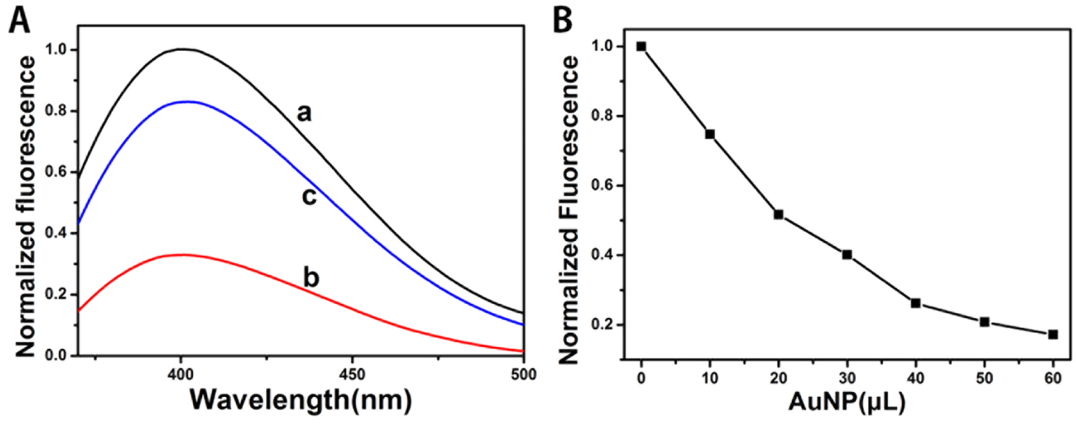

Figure 4. (A) Fluorescence emission spectra of (a) MoS_2 QDs, (b) MoS_2 QDs + HA-AuNPs, and (c) MoS_2 QDs + HA-AuNPs + HAase. (B) Effect of the amount of HA-AuNPs as quenchers on the fluorescence of the nanosystem.

shifted Z, C, and D excitonic peaks.[9,17,53] The fluorescence spectra of the QDs were measured under different excitation wavelengths. As shown in Figure 3B, the emission peak is red-shifted from 387 to 433 nm, with the excitation wavelength varying from 300 to 360 nm. The excitation-dependent fluorescence emission is consistent with other reports.[10,11,17] It may be attributed to the hot fluorescence from the K point of the Brillouin zone and the polydispersity of the MoS_2 QDs.[13,16,53] Under excitation of UV light, a blue luminescence can be easily observed by the naked eye (inset of Figure 3A). The pH-dependent fluorescence property was also studied. It can be seen in Figure S3 that the fluorescence intensity of the as-prepared QDs is relatively stable over pH values ranging from 2 to 12.

3.3. HAase Measurement. HA-AuNPs were synthesized by reducing $HAuCl_4$ with $NaBH_4$ in a HA solution. The negatively charged HA on the surface of AuNPs improves the stability and dispersion of HA-AuNPs, and a characteristic surface plasmon resonance (SPR) absorption peak around 530 nm is observed (as shown in Figure S4A, black line). The size distribution of HA-AuNPs was characterized using DLS, and the average size is about 44 nm (Figure S4B). The

DOI: 10.1021/acsami.6b01166
ACS Appl. Mater. Interfaces 2016, 8, 11272−11279

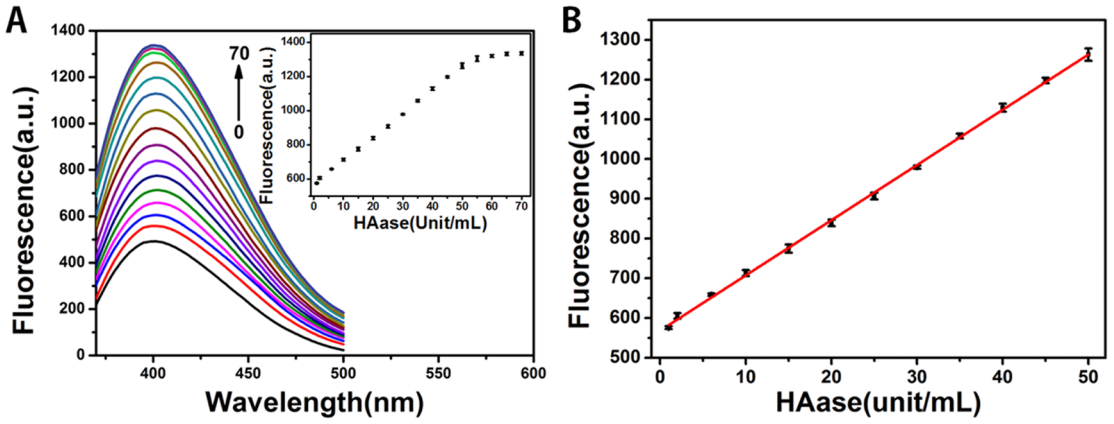

Figure 5. (A) Fluorescence spectra of MoS_2 QDs/HA-AuNPs incubated with different concentrations of HAase (0, 1, 2, 6, 10, 15, 20, 25, 30, 35, 40, 45, 50, 55, 60, 65, and 70 U/mL). The inset shows the dependence of fluorescence on the concentrations of HAase. (B) Linear plots of fluorescence versus concentrations of HAase over the range from 1 to 50 U/mL.

concentration of HA-AuNPs is about 1.0 nM based on the SPR absorption and the average DLS size of HA-AuNPs.[56] The TEM image (Figure S4C) shows that AuNPs are well-dispersed with a linear network. This might be ascribed to the linear chain structure of HA. From the TEM image of MoS_2 QDs/HA-AuNPs (Figure S4D), it can be seen that MoS_2 QDs are closely located with HA-AuNPs, indicating the formation of a nanoassembly.

The feasibility of evaluating the bioactivity of HAase is further investigated based on the MoS_2 QD/HA-AuNP nanosystem. As shown in Figure 4A, MoS_2 QDs possess strong fluorescence intensity at an excitation of 330 nm [Figure 4A(a)]. The formation of a MoS_2 QD/HA-AuNP nanoassembly leads to fluorescence quenching [Figure 4A(b)] due to electron transfer from donors (MoS_2 QDs) to acceptors (HA-AuNPs). The quenching efficacy is about 75% when 40 μL of HA-AuNPs was added to 1 mL of MoS_2 QDs (Figure 4B). The overlay of the absorption of HA-AuNPs and the fluorescence emission of MoS_2 QDs is very weak (as shown in Figure S4A), indicating that fluorescence quenching might be based on the PET mechanism. Moreover, the fluorescence lifetime of MoS_2 QDs is calculated to be 6.9 ns. After the formation of a MoS_2 QD/HA-AuNP nanoassembly, the lifetime is not changed (as shown in Figure S5), indicating that the process belongs to static quenching.

The ζ potentials for MoS_2 QDs and HA-AuNPs are about −14.5 and −22.1 mV, respectively. This indicates that there is an electrostatic repulsion interaction between the negatively charged MoS_2 QDs and HA-AuNPs. Thus, the driving force to form a nanoassembly should be other interactions. We speculate that the formation of a MoS_2 QD/HA-AuNP nanoassembly might result from coordination between the Mo atoms on the edge of the QDs and the carboxyl groups of HA[57] as well as the noncovalent interaction between Mo and N on the chain of HA. These coordinating and noncovalent interactions could overcome electrostatic repulsion between MoS_2 QDs and HA-AuNPs, leading to the formation of a nanoassembly (Figure S4D). This hypothesis was confirmed by the XPS spectra of HA-AuNPs and MoS_2 QDs/HA-AuNPs (Figure S6). Compared with the XPS survey for HA-AuNPs (Figure S6A), additional peaks of Mo and S can be observed in the XPS spectrum of MoS_2 QDs/HA-AuNPs (Figure S6B). It also indicates the formation of a nanoassembly. Moreover, the binding energies at 229.3 and 232.5 eV (Figure 2A) in the Mo 3d region for MoS_2 QDs are positively shifted to 229.7 and 232.9 eV for those of Mo 3d in MoS_2 QDs/HA-AuNPs (Figure S7). On the other hand, relative to the binding energies in the N 1s region (400.3 and 399.4 eV; Figure S6C) for HA-AuNPs, a negative shift of the binding energies (400.2 and 399.3 eV; Figure S6D) for MoS_2 QDs/HA-AuNPs is observed. The negative shift of the binding energy of N 1s and the positive shift of the binding energy of Mo 3d may be attributed to electron transfer between Mo and N due to the significant difference in the electronegativity. This is similar to the observation of noncovalent interactions between Co in a CoP nanowire and N in free nucleobases of HIV.[58]

In the presence of HAase, HA is digested into small fragments and AuNPs tend to aggregate without the protection of HA. This is confirmed by the red-shifted SPR absorption and the obvious changes of the solution color (Figure S8). Owing to the aggregation of AuNPs in the presence of HAase, electron transfer from MoS_2 QDs to AuNPs is blocked and significant recovery of the fluorescence can be observed [Figure 4A(c)]. These experimental data indicate that the measurement of HAase based on a MoS_2 QD/HA-AuNP nanoassembly is feasible. As shown in Figure 5A, quenched fluorescence of MoS_2 QDs induced by HA-AuNPs can gradually be recovered with an increase of the HAase concentration. It can be seen from the inset of Figure 5A that the fluorescence intensity reaches a plateau, while the concentration of HAase is over 55 U/mL. A linear relationship between the fluorescence intensity and concentration of HAase is obtained over the range of 1−50 U/mL (as shown in Figure 5B). The detection limit is 0.7 U/mL, which is comparable to that of a fluorescein-isothiocyanate-labeled HA-AuNP system[46] and lower than that of colorimetric assay[33,39] (Table S1).

3.4. Selectivity and Real Sample Measurements. In order to test the selectivity of the nanoprobe, various potentially interfering substances, such as inorganic salts (NaCl and KCl), small molecules [glucose (Glu), uric acid (UA), and urea], and biological macromolecules [cytochrome *c* (Cyt *c*), bovine serum albumin (BSA), and alkaline phosphatase (ALP)] were examined under the same conditions. As shown in Figure 6, the nanoprobe exhibits good selectivity.

In order to evaluate the feasibility of the proposed method in real sample detection, HAase in human urine was measured using MoS_2 QDs/HA-AuNPs as a nanoprobe through the standard addition method. Different concentrations of HAase

DOI: 10.1021/acsami.6b01166
ACS Appl. Mater. Interfaces 2016, 8, 11272−11279

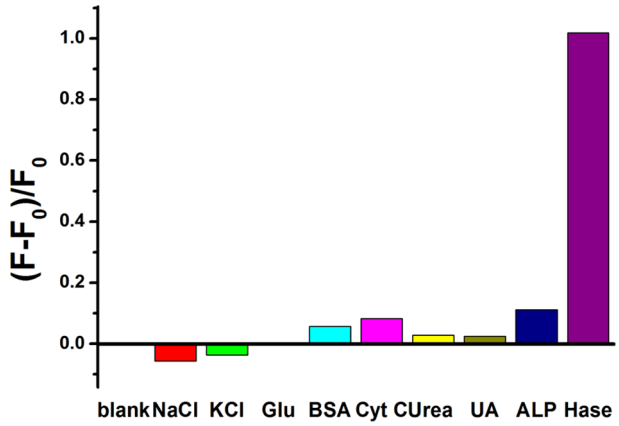

Figure 6. Fluorescence recovery of MoS_2 QDs quenched by HA-AuNPs incubated with NaCl, KCl, Glu, BSA, Cyt *c*, urea, UA, ALP, and HAase.

were added in human urine samples to prepare the spiked samples. As shown in Table 1, the recoveries are in the range of

Table 1. Determination of HAase in Urine Samples

	added HAase (U/mL)	detected HAase (U/mL)	detected HAase[a] ($\times 10^3$ mU/mg protein)	recovery (%)	RSD (n = 3, %)
1	5	5.18 ± 0.16	33.7 ± 1.0	104.6	3.16
2	25	24.19 ± 0.69	157.2 ± 4.5	96.8	2.76
3	45	44.07 ± 1.3	286.4 ± 8.6	97.9	2.93

[a]The concentration of HAase was normalized to the protein concentration in urine, which is measured to be 0.153 mg/mL with Bio-Rad protein detection kits.

96.8−104.6% with an RSD of less than 5.0%. These results indicate that the MoS_2 QDs/HA-AuNPs system can be applied for real sample measurement with satisfactory reliability.

4. CONCLUSION

In summary, we developed a one-step, bottom-up, hydrothermal route to synthesize blue fluorescent MoS_2 QDs using $(NH_4)_2MoS_4$ as the precursor. The as-prepared MoS_2 QDs exhibit a narrow lateral size distribution and good water solubility. On the basis of the PET mechanism, a sensitive and selective fluorescent probe is developed for HAase measurement using MoS_2 QDs as electron donors and HA-AuNPs as electron acceptors. The experimental results indicate that the distinct fluorescence emission of MoS_2 QDs can be utilized as a fluorescent probe for real sample analysis.

■ ASSOCIATED CONTENT

Supporting Information

The Supporting Information is available free of charge on the ACS Publications website at DOI: 10.1021/acsami.6b01166.

Raman and XPS spectra of MoS_2 QDs, pH-dependent property of MoS_2 QDs, UV−vis, DSL, and TEM of HA-AuNPs, time-resolved fluorescence spectra of MoS_2 QDs, XPS spectra of HA-AuNPs and MoS_2 QDs/HA-AuNPs, UV−vis spectra of HA-AuNPs incubating with different concentrations of HAase, and a comparison of different approaches for detection of HAase (PDF)

■ AUTHOR INFORMATION

Corresponding Authors

*E-mail: clzhang@chem.ecnu.edu.cn.
*E-mail:yzxian@chem.ecnu.edu.cn.

Notes

The authors declare no competing financial interest.

■ ACKNOWLEDGMENTS

We acknowledge financial support from the National Natural Science Foundation of China (Grant 21175046) and the Shanghai Natural Science Foundation (Grant 15ZR1411600).

■ REFERENCES

(1) Chhowalla, M.; Shin, H.; Eda, G.; Li, L.; Loh, K.; Zhang, H. The Chemistry of Two-dimensional Layered Transition Metal Dichalcogenide Nanosheets. *Nat. Chem.* **2013**, *5*, 263−275.
(2) Molina-Sánchez, A.; Wirtz, L. Phonons in Single-layer and Few-layer MoS_2 and WS_2. *Phys. Rev. B: Condens. Matter Mater. Phys.* **2011**, *84*, 1−8.
(3) Voiry, D.; Yamaguchi, H.; Li, J.; Silva, R.; Alves, D.; Fujita, T.; Chen, M.; Asefa, T.; Shenoy, V.; Eda, G.; Chhowalla, M. Enhanced Catalytic Activity in Strained Chemically Exfoliated WS_2 Nanosheets for Hydrogen Evolution. *Nat. Mater.* **2013**, *12*, 850−855.
(4) Shi, Y.; Zhou, W.; Lu, A.; Fang, W.; Lee, Y.; Hsu, A.; Kim, S.; Kim, K.; Yang, H.; Li, L.; Idrobo, J.; Kong, J. van der Waals Epitaxy of MoS_2 Layers Using Graphene as Growth Templates. *Nano Lett.* **2012**, *12*, 2784−2791.
(5) Eda, G.; Yamaguchi, H.; Voiry, D.; Fujita, T.; Chen, M.; Chhowalla, M. Photoluminescence from Chemically Exfoliated MoS_2. *Nano Lett.* **2011**, *11*, 5111−5116.
(6) Mak, K. F.; Lee, C.; Hone, J.; Shan, J.; Heinz, T. F. Atomically Thin MoS_2: A New Direct-gap Semiconductor. *Phys. Rev. Lett.* **2010**, *105*, 136805.
(7) Gopalakrishnan, D.; Damien, D.; Shaijumon, M. MoS_2 Quantum Dot-Interspersed Exfoliated MoS_2 Nanosheets. *ACS Nano* **2014**, *8*, 5297−5303.
(8) Li, Y.; Zhou, Z.; Zhang, S.; Chen, Z. MoS_2 Nanoribbons High Stability and Unusual Electronic and Magnetic Properties. *J. Am. Chem. Soc.* **2008**, *130*, 16739−16744.
(9) Splendiani, A.; Sun, L.; Zhang, Y.; Li, T.; Kim, J.; Chim, C.; Galli, G.; Wang, F. Emerging Photoluminescence in Monolayer MoS_2. *Nano Lett.* **2010**, *10*, 1271−1275.
(10) Wang, Y.; Ni, Y. Molybdenum Disulfide Quantum Dots as a Photoluminescence Sensing Platform for 2,4,6-Trinitrophenol Detection. *Anal. Chem.* **2014**, *86*, 7463−7470.
(11) Xu, S.; Li, D.; Wu, P. One-Pot, Facile, and Versatile Synthesis of Monolayer MoS_2/WS_2 Quantum Dots as Bioimaging Probes and Efficient Electrocatalysts for Hydrogen Evolution Reaction. *Adv. Funct. Mater.* **2015**, *25*, 1127−1136.
(12) Gu, W.; Yan, Y.; Cao, X.; Zhang, C.; Ding, C.; Xian, Y. A Facile and One-step Ethanol-thermal Synthesis of MoS_2 Quantum Dots for Two-photon Fluorescence Imaging. *J. Mater. Chem. B* **2016**, *4*, 27−31.
(13) Ou, J.; Chrimes, A. F.; Wang, Y.; Tang, S.; Strano, M. S.; Kalantar-zadeh, K. Ion-driven Photoluminescence Modulation of Quasi-two-dimensional MoS_2 Nanoflakes for Applications in Biological Systems. *Nano Lett.* **2014**, *14*, 857−863.
(14) Dong, H.; Tang, S.; Hao, Y.; Yu, H.; Dai, W.; Zhao, G.; Cao, Y.; Lu, H.; Zhang, X.; Ju, H. Fluorescent MoS_2 Quantum Dots: Ultrasonic Preparation, Up-Conversion and Down-Conversion Bioimaging, and Photodynamic Therapy. *ACS Appl. Mater. Interfaces* **2016**, *8*, 3107−3114.
(15) Lin, H.; Wang, C.; Wu, J.; Xu, Z.; Huang, Y.; Zhang, C. Colloidal Synthesis of MoS_2 Quantum Dots: Size-dependent Tunable Photoluminescence and Bioimaging. *New J. Chem.* **2015**, *39*, 8492−8497.

DOI: 10.1021/acsami.6b01166
ACS Appl. Mater. Interfaces 2016, 8, 11272−11279

(16) Stengl, V.; Henych, J. Strongly Luminescent Monolayered MoS_2 Prepared by Effective Ultrasound Exfoliation. *Nanoscale* **2013**, *5*, 3387−3394.
(17) Li, B.; Chen, L.; Zou, H.; Lei, J.; Luo, H.; Li, N. Electrochemically Induced Fenton Reaction of Few-layer MoS_2 Nanosheets: Preparation of Luminescent Quantum Dots via a Transition of Nanoporous Morphology. *Nanoscale* **2014**, *6*, 9831−9838.
(18) Zhang, X.; Lai, Z.; Liu, Z.; Tan, C.; Huang, Y.; Li, B.; Zhao, M.; Xie, L.; Huang, W.; Zhang, H. A Facile and Universal Top-Down Method for Preparation of Monodisperse Transition-Metal Dichalcogenide Nanodots. *Angew. Chem., Int. Ed.* **2015**, *54*, 5425−5428.
(19) Gopalakrishnan, D.; Damien, D.; Li, B.; Gullappalli, H.; Pillai, V.; Ajayan, P.; Shaijumon, M. Electrochemical Synthesis of Luminescent MoS_2 Quantum Dots. *Chem. Commun.* **2015**, *51*, 6293−6296.
(20) Qiao, W.; Yan, S.; Song, X.; Zhang, X.; He, X.; Zhong, W.; Du, Y. Luminescent Monolayer MoS_2 Quantum Dots Produced by Multi-exfoliation Based on Lithium Intercalation. *Appl. Surf. Sci.* **2015**, *359*, 130−136.
(21) Goswami, N.; Giri, A.; Pal, S. MoS_2 Nanocrystals Confined in a DNA Matrix Exhibiting Energy Transfer. *Langmuir* **2013**, *29*, 11471−11478.
(22) Ren, X.; Pang, L.; Zhang, Y.; Ren, X.; Fan, H.; Liu, S. One-step Hydrothermal Synthesis of Monolayer MoS_2 Quantum Dots for Highly Efficient Electrocatalytic Hydrogen Evolution. *J. Mater. Chem. A* **2015**, *3*, 10693−10697.
(23) Ha, H.; Han, D.; Choi, J.; Park, M.; Seo, T. Dual Role of Blue Luminescent MoS_2 Quantum Dots in Fluorescence Resonance Energy Transfer Phenomenon. *Small* **2014**, *10*, 3858−3862.
(24) Kramer, M.; Escudero, D.; Lokeshwar, S.; Golshani, R.; Ekwenna, O.; Acosta, K.; Merseburger, A.; Soloway, M.; Lokeshwar, V. Association of Hyaluronic Acid Family Members (HAS1, HAS2, and HYAL-1) with Bladder Cancer Diagnosis and Prognosis. *Cancer* **2011**, *117*, 1197−1209.
(25) Veiseh, M.; Breadner, D.; Ma, J.; Akentieva, N.; Savani, R.; Harrison, R.; Mikilus, D.; Collis, L.; Gustafson, S.; Lee, T.; Koropatnick, J.; Luyt, L.; Bissell, M.; Turley, E. Imaging of Homeostatic, Neoplastic, and Injured Tissues by HA-based Probes. *Biomacromolecules* **2012**, *13*, 12−22.
(26) Laurent, T.; Fraser, J. Hyaluronan. *FASEB J.* **1992**, *6*, 2397−2404.
(27) Lokeshwar, V.; Estrella, V.; Lopez, L.; Kramer, M.; Gomez, P.; Soloway, M.; Lokeshwar, B. HYAL1-v1, an Alternatively Spliced Variant of HYAL1 Hyaluronidase: A Negative Regulator of Bladder Cancer. *Cancer Res.* **2006**, *66*, 11219−11227.
(28) Chao, K. L.; Muthukumar, L.; Herzberg, O. Structure of Human Hyaluronidase-1, a Hyaluronan Hydrolyzing Enzyme Involved in Tumor Growth and Angiogenesis. *Biochemistry* **2007**, *46*, 6911−6920.
(29) Roberts, J.; Elder, R.; Neumann, A.; Jayaraman, A.; Bryant, S. Interaction of Hyaluronan Binding Peptides with Glycosaminoglycans in Poly(ethylene glycol) Hydrogels. *Biomacromolecules* **2014**, *15*, 1132−1141.
(30) Xie, H.; Zeng, F.; Wu, S. Ratiometric Fluorescent Biosensor for Hyaluronidase with Hyaluronan as Both Nanoparticle Scaffold and Substrate for Enzymatic Reaction. *Biomacromolecules* **2014**, *15*, 3383−3389.
(31) Zhong, Y.; Meng, F.; Deng, C.; Zhong, Z. Ligand-directed Active Tumor-targeting Polymeric Nanoparticles for Cancer Chemotherapy. *Biomacromolecules* **2014**, *15*, 1955−1969.
(32) Lokeshwar, V.; Young, M.; Goudarzi, G.; Iida, N.; Yudin, A.; Cherr, G.; Selzer, M. Identification of Bladder Tumor-derived Hyaluronidase Its Similarity to HYAL1. *Cancer Res.* **1999**, *59*, 4464−4470.
(33) Nossier, A.; Eissa, S.; Ismail, M.; Hamdy, M.; Azzazy, H. Direct Detection of Hyaluronidase in Urine Using Cationic Gold Nanoparticles: A Potential Diagnostic Test for Bladder Cancer. *Biosens. Bioelectron.* **2014**, *54*, 7−14.
(34) Benitez, A.; Yates, T.; Lopez, L.; Cerwinka, W.; Bakkar, A.; Lokeshwar, V. Targeting Hyaluronidase for Cancer Therapy: Antitumor Activity of Sulfated Hyaluronic Acid in Prostate Cancer Cells. *Cancer Res.* **2011**, *71*, 4085−4095.
(35) Martinez-Quintanilla, J.; He, D.; Wakimoto, H.; Alemany, R.; Shah, K. Encapsulated Stem Cells Loaded with Hyaluronidase-expressing Oncolytic Virus for Brain Tumor Therapy. *Mol. Ther.* **2015**, *23*, 108−118.
(36) Bouga, H.; Tsouros, I.; Bounias, D.; Kyriakopoulou, D.; Stavropoulos, M.; Papageorgakopoulou, N.; Theocharis, D.; Vynios, D. Involvement of Hyaluronidases in Colorectal Cancer. *BMC Cancer* **2010**, *10*, 499.
(37) Vercruysse, K.; Lauwers, A.; Demeester, J. Absolute and Empirical Determination of the Enzymic Activity and Kinetic Investigation of the Action of Hyaluronidase on Hyaluronan Using Viscosimetry. *Biochem. J.* **1995**, *306*, 153−160.
(38) Derrante, N. Turbidimetric Measurement of Acid Mucopolysaccharides and Hyaluronidase Activcity. *J. Biol. Chem.* **1956**, *220*, 303−306.
(39) Kim, J.; Kim, J.; Chung, S.; Chung, B. An Operationally Simple Colorimetric Assay of Hyaluronidase Activity Using Cationic Gold Nanoparticles. *Analyst* **2009**, *134*, 1291−1293.
(40) Shen, M.; Chao, C.; Wu, Y.; Wu, Y.; Huang, C.; Li, Y. A Design for Fast and Effective Screening of Hyaluronidase Inhibitor Using Gold Nanoparticles. *Sens. Actuators, B* **2013**, *181*, 605−610.
(41) Steiner, B.; Cruce, D. A Zymographic Assay for Detection of Hyaluronidase Activity on Polyacrylamide Gels and Its Application to Enzymatic Activity Found in Bacteria. *Anal. Biochem.* **1992**, *200*, 405−410.
(42) Delpech, B.; Bertrand, P.; Maingonnat, C.; Girard, N.; Chauzy, C. Enzyme-linked Hyaluronectin A Unique Reagent for Hyaluronan Assay and Tissue Location and for Hyaluronidase Activity Detection. *Anal. Biochem.* **1995**, *229*, 35−41.
(43) Fudala, R.; Mummert, M.; Gryczynski, Z.; Gryczynski, I. Fluorescence Detection of Hyaluronidase. *J. Photochem. Photobiol., B* **2011**, *104*, 473−477.
(44) Rich, R.; Mummert, M.; Foldes-Papp, Z.; Gryczynski, Z.; Borejdo, J.; Gryczynski, I.; Fudala, R. Detection of Hyaluronidase Activity Using Fluorescein Labeled Hyaluronic Acid and Fluorescence Correlation Spectroscopy. *J. Photochem. Photobiol., B* **2012**, *116*, 7−12.
(45) Chib, R.; Raut, S.; Fudala, R.; Chang, A.; Mummert, M.; Rich, R.; Gryczynski, Z.; Gryczynski, I. FRET Based Ratio-Metric Sensing of Hyaluronidase in Synthetic Urine as a Biomarker for Bladder and Prostate Cancer. *Curr. Pharm. Biotechnol.* **2013**, *14*, 470−474.
(46) Cheng, D.; Han, W.; Yang, K.; Song, Y.; Jiang, M.; Song, E. One-step Facile Synthesis of Hyaluronic Acid Functionalized Fluorescent Gold Nanoprobes Sensitive to Hyaluronidase in Urine Specimen From Bladder Cancer Patients. *Talanta* **2014**, *130*, 408−414.
(47) Wang, Z.; Li, X.; Song, Y.; Li, L.; Shi, W.; Ma, H. An Upconversion Luminescence Nanoprobe for the Ultrasensitive Detection of Hyaluronidase. *Anal. Chem.* **2015**, *87*, 5816−5823.
(48) Liu, S.; Zhao, N.; Cheng, Z.; Liu, H. Amino-functionalized Green Fluorescent Carbon Dots as Surface Energy Transfer Biosensors for Hyaluronidase. *Nanoscale* **2015**, *7*, 6836−6842.
(49) Roy, P.; Srivastava, S. Chemical Bath Deposition of MoS_2 Thin Film Using Ammonium Tetrathiomolybdate as a Single Source for Molybdenum and Sulphur. *Thin Solid Films* **2006**, *496*, 293−298.
(50) Song, E.; Li, J.; Wei, H.; Song, Y. One-step Facile Synthesis of N-acetylglucosamine-functionalized Gold Nanoparticles for Direct Visual and Light-scattering Detection of Lectin from Wheat Germ. *Anal. Methods* **2012**, *4*, 1199−1201.
(51) Gan, Z.; Liu, L.; Wu, H.; Hao, Y.; Shan, Y.; Wu, X.; Chu, P. Quantum Confinement Effects across Two-dimensional Planes in MoS_2 Quantum Dots. *Appl. Phys. Lett.* **2015**, *106*, 233113.
(52) Liu, Y.; Nan, H.; Wu, X.; Pan, W.; Wang, W.; Bai, J.; Zhao, W.; Sun, L.; Wang, X.; Ni, Z. Layer-by-Layer Thinning of MoS_2 by Plasma. *ACS Nano* **2013**, *7*, 4202−4209.

DOI: 10.1021/acsami.6b01166
ACS Appl. Mater. Interfaces 2016, 8, 11272−11279

(53) Wang, Y.; Ou, J.; Balendhran, S.; Chrimes, A.; Mortazavi, M.; Yao, D.; Field, M.; Latham, K.; Bansal, V.; Friend, J.; Zhuiykov, S.; Medhekar, N.; Strano, M.; Kalantar-zadeh, K. Electrochemical Control of Photoluminescence in Two-dimensional MoS_2 Nanoflakes. *ACS Nano* **2013**, *7*, 10083−10093.
(54) Lee, C.; Yan, H.; Brus, L. E.; Heinz, T. F.; Hone, J.; Ryu, S. Anomalous Lattice Vibrations of Single and Few Layer MoS_2. *ACS Nano* **2010**, *4*, 2695−2700.
(55) Matte, H. S.; Gomathi, A.; Manna, A. K.; Late, D. J.; Datta, R.; Pati, S. K.; Rao, C. N. MoS_2 and WS_2 Analogues of Graphene. *Angew. Chem., Int. Ed.* **2010**, *49*, 4059−4062.
(56) Haiss, W.; Thanh, N. T. K.; Aveyard, J.; Fernig, D. G. Determination of Size and Concentration of Gold Nanoparticles from UV−Vis Spectra. *Anal. Chem.* **2007**, *79*, 4215−4221.
(57) Zhou, Z.; Wan, H.; Tsai, K. Syntheses and Spectroscopic and Structural Characterization of Molybdenum(VI) Citrato Monomeric Raceme and Dimer, $K_4[MoO_3(cit)]\ 2H_2O$ and $K_4[(MoO_2)_2O(Hcit)_2]\ 4H_2O$. *Inorg. Chem.* **2000**, *39*, 59−64.
(58) Tian, J.; Cheng, N.; Liu, Q.; Xing, W.; Sun, X. Cobalt Phosphide Nanowires: Efficient Nanostructures for Fluorescence Sensing of Biomolecules and Photocatalytic Evolution of Dihydrogen from Water under Visible Light. *Angew. Chem., Int. Ed.* **2015**, *54*, 5493−5497.

DOI: 10.1021/acsami.6b01166
ACS Appl. Mater. Interfaces 2016, 8, 11272−11279